Bi-directionally Efficient, Backdrivable Gearbox with Low Backlash for Robot Actuators

Wonseok Shin[1], Bummo Ahn[1], and Suncheol Kwon[1]

[1]Affiliation not available

January 17, 2025

Bi-directionally Efficient, Backdrivable Gearbox with Low Backlash for Robot Actuators

Wonseok Shin, Bummo Ahn, and Suncheol Kwon

***Abstract*—This article presents a design framework for a back-drivable, bi-directionally energy-efficient 3K compound gearbox with a high reduction ratio and low backlash. The 3K compound planetary gearbox is a promising candidate for the robot actuators deployed in physically interacting environments possessing a compact design with a high gear ratio and high back-drivability. However, the existing 3k composite planetary gearbox has a high backlash for use in robot actuators. In this context, the proposed design framework comprises 1) backlash modeling 2) effective inertia of the 3K compound planetary gearbox 3) maximization of the bi-directional efficiency under bounded backlash constraints. We created a prototype to demonstrate the design framework for a low-backlash gearbox with a high reduction ratio (1/96.2) which is both bi-directionally efficient and back-drivable. The angular backlash of the prototype was 7.1 arcminutes. The forward and backward efficiencies of the developed prototype were 87.1 % and 82.5 %, respectively, and the back-driving starting torque was 0.025 Nm.**

***Index Terms*— Robot Actuators, Compound Planetary Gearbox, High-Reduction Ratio, Low Backlash, Bi-Directionally Efficient**

I. INTRODUCTION

NOWADAYS, robots are being used beyond industrial sites, expanding their application range to various environments where they physically coexist with humans [1], [2]. This trend address the significant issue of robot actuator performance for the coexistence and interaction with humans. In most robotic applications, an electric motor is essentially paired with a gearbox to achieve the required high torque capacity [3]. Various gearboxes, such as multi-stage planetary gears [4], strain wave gears (harmonic drives) [5], and cycloidal drives, are used in robots, offering high precision characterized by low backlash and high torque-to-weight ratios [6]. Gearboxes with reduction ratios ranging from approximately 5:1 to 300:1 are also appropriately utilized depending on the application.

Increasing the reduction ratio of a gearbox enhances stiffness and amplifies energy, thereby increasing the magnitude of forward transmission energy that drives the robot, but simultaneously decreasing backdrivability dramatically due to high mechanical impedance [7]. A high reduction ratio gearbox with an integrated torque sensor can be used to improve backdrivability and facilitate stable interactions by detecting external torque and disturbance [8]. Although torque sensor-based control allows for backdrivability in high mechanical impedance actuators, the system's performance is significantly influenced by the sensor's bandwidth, resulting in a limited control bandwidth [9]. In other words, a gearbox with a high reduction ratio and high backdrivability is a promising solution for robot actuators in physical interaction applications.

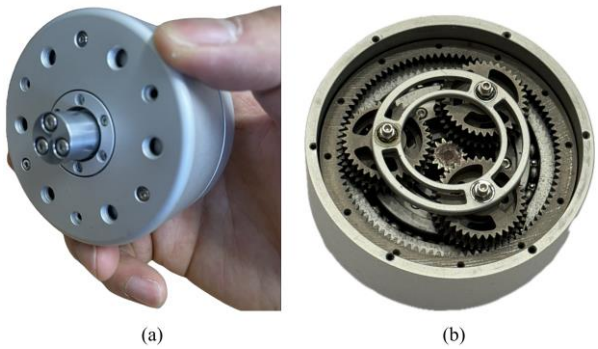

Fig. 1. (a) The exterior and (b) the internal structure of the proposed 3K compound planetary gearbox

Recently, a 3K compound planetary gearbox design has been proposed to overcome the shortcomings of traditional multi-stage planetary gearboxes, featuring a high gear ratio while simultaneously maximizing efficiency in both drive directions [10]. The gearbox design can be outlined in two steps: 1) establishing the analytic relationship between forward and backward direction efficiency using kinematics and dynamics of the energy transmission, and 2) maximizing the efficiency in both directions. In comparison to a harmonic drive with a similar gear ratio, the compound planetary gearbox demonstrated greater efficiency in both directions and significantly lower backdriving torque. However, the proposed gear exhibited a high backlash of 24 arcmin, which restricts the robot control accuracy.

To address the issue of high backlash while preserving high energy efficiency in both drive directions, Oba et al. [11] introduced a hybrid design combining a traction drive with a 3K compound planetary gearbox. The traction drive transmits power through the rolling contact using the roller instead of gear teeth. The proposed design lowered the backlash to less than 1.2 arcmin and improved efficiency by 90%. However, for using as a gearbox, little is known about the durability of roller-based power transmission, and further research is required to

This work was supported in part by the Technology Innovation Program, Development of Safe and Comfortable Human Augmentation Hybrid Robot Suit, funded by the Ministry of Trade, Industry, and Energy (MOTIE), South Korea, under Grant 20007058.

Wonseok Shin, Bummo Ahn, and Suncheol Kwon are with the Human-Centric Robotics Research and Development Department, the Korea Institute of Industrial Technology, Sangnok-gu, Ansan, 15588, Republic of Korea. Corresponding author is Suncheol Kwon (skwon@kitech.re.kr).

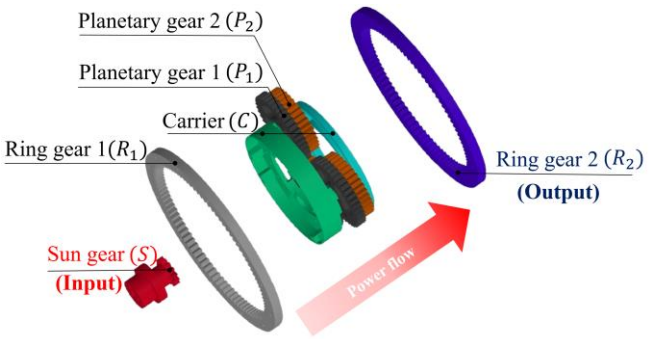

Fig. 2. The configuration of the proposed gearbox

TABLE I
NOMENCLATURE OF VARIABLES

Parameters	Contents
z_S	Number of teeth of S
z_{P_1}	Number of teeth of P_1
z_{R_1}	Number of teeth of R_1
z_{P_2}	Number of teeth of P_2
z_{R_2}	Number of teeth of R_2
m_1	Gear module of first stage
m_2	Gear module of second stage
x_S	Profile shift coefficient of S
x_{P_1}	Profile shift coefficient of P_1
x_{R_1}	Profile shift coefficient of R_1
x_{P_2}	Profile shift coefficient of P_2
x_{R_2}	Profile shift coefficient of R_2
α_{s1}	Starting angle of the S
α_{s2}	Starting angle of the P_1
α_{s3}	Starting angle of the R_1
d_1	Center distance between gear pair of first stage
d_2	Center distance between gear pair of second stage
α_{w1}	Working pressure angle of meshing pair 1 (S-P_1)
α_{w2}	Working pressure angle of meshing pair 2 (P_1-R_1)
α_{w3}	Working pressure angle of meshing pair 3 (P_2-R_2)

address the durability of roller-based power transmission. In a similar effort, Kawamoto [12] developed a planetary roller-type traction drive with a very low backlash to less than 4 arcsec, surpassing what is possible with conventional gear designs. However, the very low torque capacity restricts its use in robotic applications [13].

In this paper, we present a gearbox designed for robot actuators, featuring a high reduction ratio, bi-directionally efficient, high backdrivability and low backlash. Inspired by previous literature on the highly back-drivable gearbox [10], we investigated the in-depth model of backlash and bidirectional efficiency in the 3K compound planetary gearbox. The efficiency of the gearbox is known as influenced by four key factors: 1) the number of teeth, 2) the profile shift coefficient, 3) the gear module, and 4) the center distance between the gear teeth. Based on these observations, we present a gearbox design framework that maximizes gear efficiency while maintaining backlash within the bounded backlash. We established the required backlash boundary based on the backlash performance of commercially used quasi-direct drives (QDDs), which have been widely used in robotic applications that interact with the human and the external environment [14-16]. Commercial QDDs developed for robot joints exhibit a backlash of

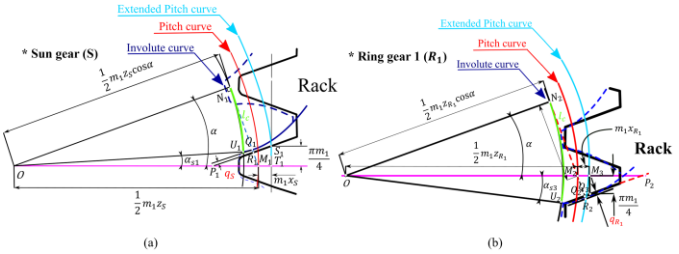

Fig. 3 (a) Spur gear generation (Especially, S) and (b) internal gear generation using rack cutting (Especially, R_1). Machining allowance of each case is expressed as q_s and q_{R_1} respectively in red.

approximately 10 arc-minutes [17].

The remainder of this study is organized as follows: Section II provides the in-depth modeling of the backlash of the 3K compound planetary gearbox. Section III provides the effective inertia of the 3K compound planetary gearbox. Section IV describes the simulation for optimal gearbox design, and Section V describes the experimental result of the power efficiency, back-drivability, and backlash. Section VI discusses and conclude the performance of the developed gear design.

II. BACKLASH MODEL OF THE GEARBOX

The backlash of the proposed 3K compound planetary gearbox is determined by the combination of spaces between each meshing gear pair. The backlash was classified into two categories: between two separate spur gears and between the spur gear and the internal gear. As an example of the first category, we introduce S and P_1 for the explanation of category 1. Likewise, P_1 and R_1 are used as an example of the second category (see Fig 2). The terms related to backlash used here are specified with reference to the contents of ISO 21771 [18]. We denoted variables used in the modeling as shown in Table I.

A. Machining allowance and backlash

ISO 21771 states that a roughing gear-cutting tool leaves a machining allowance, q, on the flank of the cylindrical gear for the finishing process [18]. This machining allowance is specified perpendicular to the tooth surface and known to be a one of the contributing factor of the normal backlash, j_{bn}, see Fig. 3. Although backlash is influenced not only by machining tolerances, q but also by elemental tolerances such as profile, helix, and runout, this study focuses on the machining allowance, q to develop an in-depth modeling of backlash. We assume that the machining allowance is one of the independent variables contributing to the backlash.

B. Normal backlash between spur gears

Fig. 4 (a) represents the configuration of the gear meshing between two distinct spur gears. The backlash ($\overline{P_1P_2}$) can be derived through an analysis of the length of the external common tangent of each base circle ($\overline{BP_3}$), as expressed in the following equations.

$$\overline{O_1O_2}\sin\alpha_{w1} = \overline{BP_3} = \overline{BP_1} + \overline{P_1P_2} + \overline{P_2P_3} \quad (1)$$

$$\overline{BP_1} = \widehat{BC} + \widehat{CF} = 0.5m_1z_S\cos\alpha(\alpha + \gamma_1 - \alpha_{s1}) \quad (2)$$

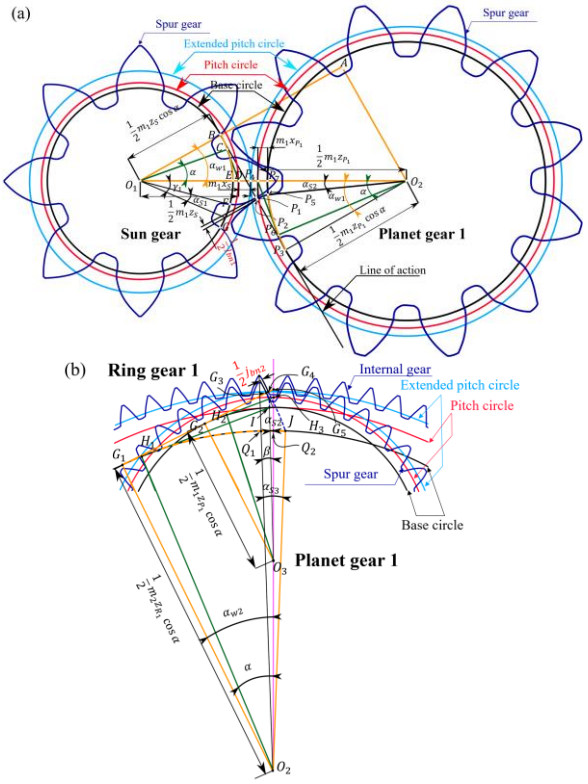

Fig. 4 (a) Backlash configuration between two distinct spur gears (Especially, S-P_1) and (b) between spur gear and internal gear (Especially, P_1-R_1)

$$\overline{P_2P_3} = \widehat{P_3P_5} = 0.5m_1z_{P_1}\cos\alpha(\alpha_{w1} - \alpha_{s2}) \tag{3}$$

where $\overline{P_1P_2} = 0.5j_{bn1}$ and $\gamma_1 = 2\pi/2Z_S$.
Fig. 4 (a) depicts the backlash produced during the rack cutting process for the spur gears (especially, S). From the geometric analysis, we can derive the following equation.

$$\overline{Q_1R_1} = \overline{M_1N_1} - \overline{M_1R_1} - \overline{N_1Q_1} \tag{4}$$

where $\overline{M_1N_1} = 0.5m_1z_S\sin\alpha$, $\overline{M_1R_1} = (m_1\pi\cos\alpha/4\sin\alpha - m_1x_S)\sin\alpha$, and $\overline{N_1Q_1} = \widehat{N_1U_1} = \frac{1}{2}m_1z_S\cos\alpha\,(\alpha - \alpha_{s1})$.
By rearranging the above equation (22), the root starting angle of spur gear (Fig. 4 (a)) denoted by α_{s1} and α_{s2} can be described as follows.

$$\alpha_{s1} = \alpha + \frac{\pi}{2z_S} + \frac{q_S}{z_S\cos\alpha} - \left(1 + \frac{2x_S}{z_S}\right)\frac{\sin\alpha}{\cos\alpha} \tag{5}$$

$$\alpha_{s2} = \alpha + \frac{\pi}{2z_{P_1}} + \frac{q_{P_1}}{z_{P_1}\cos\alpha} - \left(1 + \frac{2x_{P_1}}{z_{P_1}}\right)\frac{\sin\alpha}{\cos\alpha} \tag{6}$$

where q_S and q_{P_1} are machining allowance of S and P_1.

C. Normal backlash between a spur gear and an internal gear

Fig 4. (b) represents the meshing interaction between the planet gear and the internal gear. The linear backlash ($\overline{G_3G_4}$) was calculated based on the length of the external common tangent of each base circle ($\overline{G_1G_2}$), as expressed in the following equations.

$$\overline{O_2O_3}\sin\alpha_{w2} = \overline{G_1G_2} = \overline{G_1G_4} - \overline{G_2G_4} \tag{7}$$

$$\begin{aligned}\overline{G_1G_4} &= \widehat{G_1J} = \widehat{G_1H_1} + \widehat{H_1Q_2} + \widehat{Q_1J} - \widehat{Q_1Q_2} \\ &= 0.5\,m_1z_{R_1}(\alpha_{w2} + \alpha_{s3} - \beta)\cos\alpha\end{aligned} \tag{8}$$

$$\overline{G_2G_4} = 0.5m_1z_2\cos\alpha(\alpha_{w2} - \alpha_{s2}) + 0.5j_{bn2} \tag{9}$$

In a manner similar to the spur gear generation, the internal gear generation using rack cutting is illustrated in Fig. 3 (b) (especially, R_1). The detailed backlash from the manufacturing the internal gear is derived in following equations.

$$\begin{aligned}\overline{Q_2R_2} = 0.5m_1z_{R_1}\cos\alpha(\alpha + \alpha_{s3}) - 1.5m_1z_{R_1}\sin\alpha \\ - 0.25m_1\pi\cos\alpha\end{aligned} \tag{10}$$

$$\overline{M_2P_2} = m_1x_{R_1} + m_1\pi\cos\alpha/4\sin\alpha \tag{11}$$

Similar to (5) and (6), by rearranging the above equation (8), the root starting angle denoted by α_{s3} is given by following equations

$$\alpha_{s3} = -\alpha + \frac{\pi}{2z_{R_1}} + \frac{q_{R_1}}{Z_{R_1}\cos\alpha} + \left(1 + \frac{2x_{R_1}}{z_{R_1}}\right)\frac{\sin\alpha}{\cos\alpha} \tag{12}$$

where q_{R_1} is a machining allowance of R_1, see Fig. 4 (b).

D. Total backlash angle

Based on the previously derived relations analysis (1) to (12), the normal backlash in each gear pair engagement can be calculated. We detailed three normal backlash in each gear meshing, as represented by the following equations.

$$\begin{aligned}j_{bn1} = 2d_1\sin\alpha_{w1} - m_1\left(z_S + z_{P_1}\right)\cos\alpha(\alpha_{w1} - \alpha) \\ -m_1\left(z_S + z_{P_1} + 2x_S + 2x_{P_1}\right)\sin\alpha + m_1(q_S + q_{P_1})\end{aligned} \tag{13}$$

$$\begin{aligned}j_{bn2} = -2d_2\sin\alpha_{w2} - m_1\left(z_{P_1} - z_{R_1}\right)\cos\alpha(\alpha_{w2} - \\ \alpha) - m_1\left(z_{P_1} - z_{R_1} + 2x_{P_1} - 2x_{R_1}\right)\sin\alpha + \\ m_1(q_{P_1} + q_{R_1})\end{aligned} \tag{14}$$

(25)

$$\begin{aligned}j_{bn3} = -2d_2\sin\alpha_{w3} - m_2\left(z_{P_2}\right. \\ \left. - z_{R_2}\right)\cos\alpha(\alpha_{w3} - \alpha) \\ - m_2\left(z_{P_2} - z_{R_2} + 2x_{P_2}\right. \\ \left. - 2x_{R_2}\right)\sin\alpha + m_2(q_{P_2} + q_{R_2})\end{aligned} \tag{15}$$

where q_S, q_{P_1}, q_{R_1}, q_{P_2}, and q_{R_2} represent the machining allowance of the S, P_1, R_1, P_2, and R_2, respectively (refer to ISO 21771 7.2 [18]), and j_{bn1}, j_{bn2}, j_{bn3} are the linear backlash between three different gear meshing conditions.
In our previous study [19], we presented a backlash angle derived from the combination of the obtained normal backlash and the effective radius of each gear meshing, ε_i as follows:

$$\varphi_i = \frac{j_{bni}}{\cos\alpha} \cdot \frac{180}{\pi\varepsilon_i}, i \in \{1,2,3\} \quad (16)$$

We simply added each of the three backlash angles. However, this approach didn't account for the gear power transmission principles, resulting in an error that produced backlash predictions larger than the actual values.

Once the input sun gear engages with P_1 (stage 1), power is transferred, causing the connected P_2 to rotate the output R_2 (stage 2), completing the power transmission. Therefore, the backlash in the first stage (φ_1) is inevitably included in the total backlash as is. In the second stage, since P_1 and P_2 are coupled, power can be finally transmitted to the output side if only R_1, R_2, and the large clearance between them rotate. We combine the two backlashes from stage 1 and stage 2 to estimate the total backlash. The following equation express the estimated total backlash (φ_T),

I

$$\varphi_T = \varphi_1 + \max(\varphi_2, \varphi_3) \quad (17)$$

III. Effective Inertia of The Gearbox

This section describes the backdrivability of the proposed 3K compound planetary gearbox. We provide modeling of the effective inertia by leveraging the derivation of effective inertia during forward and backward drives of a gear pair (III-A), analyze the kinematics (III-B), and applying these to the proposed gear design (III-C).

A. Power balance in gear drive

Previous literatures [10], [20] reported that the power efficiency is determined through the analysis of the kinematic layout and dynamics-based power balance equations, considering factors such as the number of gear teeth, module, profile shift coefficient, center distance between each gear pair, and friction coefficient, as follows.

$$\eta_f = \frac{(1+\eta_{SP_1}\eta_{P_1R_1}G_1)(1-G_2)}{(1-\eta_{P_1R_1}\eta_{P_2R_2}G_1)(1+G_1)} \quad (18)$$

$$\eta_b = \frac{\eta_{SP_1}(1+G_1)(\eta_{P_1R_1}\eta_{P_2R_2}-G_2)}{\eta_{P_2R_2}(G_1+\eta_{SP_1}\eta_{P_1R_1})(1-G_2)} \quad (19)$$

Fig. 5 represents the gear meshing configuration between the driving gear and driven gear, through which the power balance relation can be derived as follows:

1) Forward driving: During the forward driving, the driving power flows is transmitted to the driven gear considering the forward power efficiency, η_f and the dynamic relation is derived as below (see Fig. 5 (a)).

$$J_2\alpha_2 = \eta_f i(\tau_1 - J_1\alpha_1) - \tau_2 \quad (20)$$

where i is the reduction ratio between driving gear and driven gear ($i = w_1/w_2$), J_1 and J_2 are the moment of inertia of the driving and driven gear, τ_1 and τ_2 are the torque of the driving and driven gear, $\alpha_1 = \frac{dw_1}{dt}$ and $\alpha_2 = \frac{dw_2}{dt}$ are the angular acceleration of the driving and driven gear.

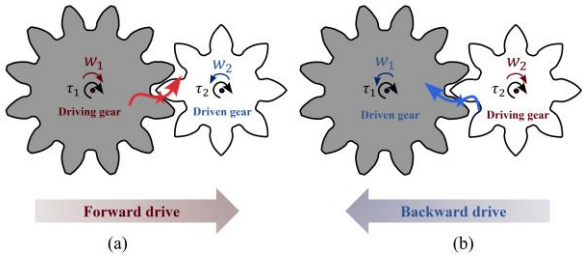

Fig. 5. Gear meshing concept of both (a) forward and (b) backward drive. τ_1 and w_1 are the torque and angular velocity vector of the driving gear of the forward drive. τ_2 and w_2 are the torque and angular velocity vector of the driving gear during the backward drive.

By multiplying w_2 on both sides of the (20) and rearranging the equation (21) the following power balance relation (22) is derived.

$$J_2\alpha_2 w_2 = \eta_f(\tau_1 w_1 - J_1\alpha_1 w_1) - \tau_2 w_2 \quad (21)$$

$$\frac{d}{dt}\left(\frac{1}{2}J_2 {w_2}^2\right) + \tau_2 w_2 = \eta_f\left(\tau_1 w_1 - \frac{d}{dt}\left(\frac{1}{2}J_1 {w_1}^2\right)\right) \quad (22)$$

From the perspective of the driving gear, the relation (22) can be expressed in terms of the effective moment of inertia of the forward drive.

$$\tau_2 w_2 = \eta_f\left(J_1 w_1 - \frac{d}{dt}\left(\frac{1}{2}\tilde{J}_f {w_1}^2\right)\right) \quad (23)$$

where $\tilde{J}_f$ is the effective moment of inertia of the forward drive. Combining the relation (22) and (23), the effective moment of inertia of the forward driving is inversely proportional to both the square of the reduction ratio, i and forward driving efficiency, η_f as follows:

$$\tilde{J}_f = J_1 + J_2/i^2\eta_f \quad (24)$$

2) Backward drive: In the case of backward driving, the angular velocity vector of the driving gear has the opposite sign to the driven gear in forward driving, as does the angular acceleration vector (Fig. 5 (b)). As with forward driving, backward driving dynamics can be expressed as follows by utilizing backward driving efficiency, η_b.

$$J_2(-\alpha_2) = \tau_2 - i\big(\tau_1 + (-J_1\alpha_1)\big)/\eta_b \quad (25)$$

In the same manner as forward driving, the backward power balance relation (27) is derived by multiplying the $w_2$on both sides of the relation (25) and rearranging the relation (26).

$$J_2(-\alpha_2)w_2 = \tau_2 w_2 - (\tau_1 w_1 - J_1\alpha_1 w_1)/\eta_b \quad (26)$$

$$\frac{d}{dt}\left(\frac{1}{2}J_2 {w_2}^2\right) + \tau_2 w_2 = \frac{1}{\eta_b}\left(\tau_1 w_1 - \frac{d}{dt}\left(\frac{1}{2}J_1 {w_1}^2\right)\right) \quad (27)$$

From the perspective of the driven gear, the relation (27) can be summarized in terms of the effective moment of inertia of the backward drive.

$$\tau_1 w_1 = \eta_b \left(J_2 w_2 + \frac{d}{dt}\left(\frac{1}{2}\tilde{J}_b {w_2}^2\right)\right) \tag{28}$$

where $\tilde{J}_b$ is the effective moment of inertia of the backward drive. Combining the relation (27) and (28), the effective moment of inertia of the backward driving is proportional to both the square of the reduction ratio, i and inversely proportional to the forward driving efficiency, η_b as follows:

$$\tilde{J}_b = \frac{i^2}{\eta_b} J_1 + J_2 \tag{29}$$

From the (29), we can infer that the higher η_b leads the higher the backdrivability.

B. Kinematics

In the proposed 3K compound planetary gearbox, power is transmitted at three gear mesh points: between the S and P_1, between P_1 and R_1, and between P_2 and R_2.

Each planetary motion can be broken down into a rolling motion combined with a coupled motion. This can be mathematically represented as follows:

$$w_G = w'_G + w_C \tag{30}$$

where w_G and w'_G represent the absolute and rolling angular velocities of the gear in each planetary gearbox. Here, the rolling angular velocity, w'_G affects the power transmission efficiency in each meshing gear pair by contributing to power losses resulting from friction between the gear teeth.

Based on the Willis relation [20] in each gear meshing, the total gear ratio of the proposed 3K compound planetary gearbox is summarized as follow:

$$i_T = \frac{w'_S}{w'_{R_2}} = \frac{1 + G_1}{1 - G_2} \tag{31}$$

where i_T denotes the gear ratio of the total transmission, and $G_1 = z_{R_1}/z_S$, $G_2 = z_{P_2} z_{R_1}/z_{P_1} z_{R_2}$.

C. Effective inertia

The effective moment of inertia contributes to the backdrivability performance of the proposed compound planetary gearbox. Using the effective moment of inertia derived in the previous section (29), we applied this concept to the 3K compound planetary gear to determine its effective inertia. From the perspective of the driven gear in each case, the effective moment of inertia can be organized as follows based on equation (29).

To quantitatively assess the backdriving performance of the compound planetary gearbox, it is necessary to convert the effective inertia to the angular velocity of ring gear 2 (w_2) which is the angular velocity of the output stage. The backward effective inertia of the output stage can be formulated as shown below.

$$\tilde{J}_{3K} = \frac{i_{SR_2}^2}{\eta_{SP_1}\eta_{P_1R_1}} J_S + \frac{3 i_{P_1R_2}^2}{\eta_{P_1R_1}} J_{P_1} + \frac{3 i_{P_2R_2}^2}{\eta_{P_2R_2}} J_{P_2} + J_{R_2} + i_{CR_2}^2 \tilde{J}_C \tag{32}$$

$$\tilde{J}_C = J_C + 3(J_{P_1} + J_{P_2} + m_P \cdot {r_C}^2) \tag{33}$$

where $i_{SR_2} = w'_S/w'_{R_2}$, $i_{P_1R_2} = w'_{P_1}/w'_{R_2}$, and $i_{CR_2} = w'_C/w'_{R_2}$ denote the rolling angular velocity ratio between S and R_2, $P_1$and R_2, C and R_2, and P_2 and R_2, respectively. $\tilde{J}_C$ denote the moment of inertia of the C and P_1 with P_2 using parallel-axis theorem, J_C denote the moment of inertia of the carrier, m_P denote the mass of both P_1 and P_2, and r_C is the center distance of the P_1. η_{SP_1}, $\eta_{P_1R_1}$, and $\eta_{P_2R_2}$ denote the respective driving efficiency during rolling in each gear meshing pairs.

IV. Optimization

Hiroshi *et al*. [10] reported that when the forward-driving efficiency was optimized, the backward-driving efficiency was also optimized. Therefore, we have chosen the following strategy. We investigated the efficiency trends by defining the range of the backlash boundary and maximizing the efficiency using an exhaustive search method. The formulated optimization problem is described as follows:

$$\max \eta_b(z_S, z_{P_1}, z_{R_1}, z_{P_2}, z_{R_2}, x_S, x_{P_1}, x_{R_1}, x_{P_2}, x_{R_2}, m_1, m_2) \tag{34}$$

$$\text{subject to } 0 \le x_j \le x_U, j \in \{S, P_1, R_1, P_2, R_2\} \tag{35}$$

$$1 \le \epsilon_i \le 2, i \in \{1,2,3\} \tag{36}$$

$$\varphi_L \le \varphi_T \le \varphi_U \tag{37}$$

where x_j and m_i are the profile shift coefficient and the module of each gear, x_U and φ_U are upper bound of profile shift coefficient of each gear and total angular backlash, respectively, and ϵ_i is the contact ratio of the gear meshing.

We carried out the gearbox design using a framework consisting of the following steps.

1) Set the upper and lower boundary of the target reduction ratio of the gearbox.
2) Execute exhaustive search for the gear teeth numbers.
    a) Calculate the total gear ratio and the backlash using the selected gear teeth number with a zero profile shift coefficient
    b) Calculate the corresponding power efficiency with a zero profile shift coefficient
    c) Select the combination of the gear teeth number satisfying the required gear ratio and the minimum backlash
3) Set the upper and lower boundary of the profile shift coefficient and module.
4) Maximize the efficiency by applying the sequential quadratic programming algorithm to every feasible solution identified in the exhaustive search.

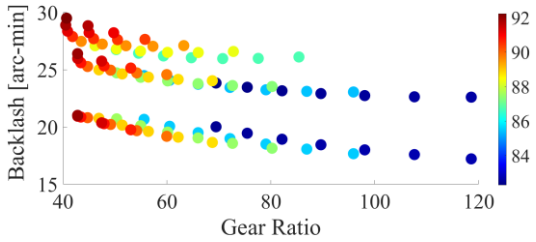

Fig. 6. Relations between gear ratio and backlash with backward efficiency (zero profile shift coefficient condition) from the simulation result. Color bar represents the backward efficiency [%]

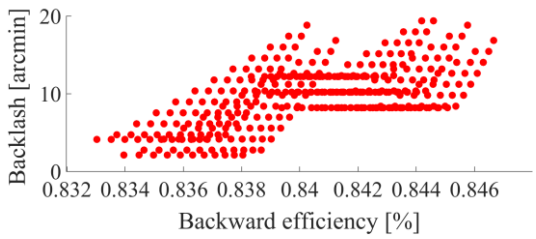

Fig. 7. Relations between the backward efficiency and the backlash (profile shifted condition) from the simulation result.

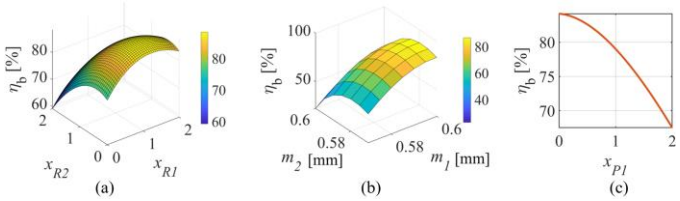

Fig. 8. Simulated backward efficiency, η_b of the optimization. (a) Backward efficiency with respect to the profile shift coefficients of the R_1, R_2 (x_{R_1}, x_{R_2}). (b) Backward efficiency with respect to the module (m_1, m_2). (c) Backward efficiency with respect to the profile shift coefficient of the P_1 (x_{P_1}).

5) Choose the best solution of the maximum efficiency within the constraint backlash condition satisfying the assembly condition.

The efficiency maximization problem we aim to solve above falls into the category of constrained nonlinear optimization problems. A sequential quadratic programming (MATLAB's *fmincon* function) was implemented to find the maximum efficiency within the bounded backlash [21]. We accomplished the equivalent of maximizing the efficiency function, as outlined in Equation (34), by negating the efficiency function, η_b (multiplying it by -1) and then addressing the problem of minimizing the resulting value.

We performed a simulation to expect the performance of the prototype and evaluate the proposed modeling and optimization algorithm. First, we analyzed the relationship between the gear ratio and backlash according to changes in the tooth number combination, following processes 1) and 2) under the zero profile shift coefficient and the module satisfying the outer diameter approximately 80 mm. Especially, we selected a gear tooth combination matching the reduction ratio 96.2:1 established in literature [10] under identical reduction ratio conditions to evaluate the backlash improvement effect using the proposed backlash modeling, see Fig. 6. From the result of the exhaustive search, we examined the backlash changes according to the gear ratio and the backward efficiency at the corresponding points, see Fig. 7.

TABLE II
SPECIFICATION OF THE GEARBOX

Parameters	Proposed	Bilateral drive [10]
z_S	14	12
z_{P_1}	40	39
z_{R_1}	94	90
z_{P_2}	36	32
z_{R_2}	92	81
x_S	0.5	0.476
x_{P_1}	0	0.762
x_{R_1}	0.45	2.000
x_{P_2}	0.4	0.526
x_{R_2}	0.29	1.210
m_1	0.59 mm	0.8 mm
m_2	0.58 mm	0.8467 mm
α	20 °	20 °

Subsequently, we applied the profile shift coefficient to assess the extent of backlash improvement compared to the case without its application, while also analyzing its impact on efficiency. The results showed that the backlash could be reduced from around 18 arcmin to 2 arcmin, with the backdriving efficiency in this configuration reaching approximately 89%, see Fig. 8 (a). With all other conditions fixed, we checked the backward efficiency as the module changed and verified that it peaked within a highly localized range, see Fig 8 (b). When only the profile shift coefficient x_{P_1} is varied while all other variables remain constant, the optimization problem demonstrates convexity, as depicted in Fig. 8 (c). Based on these simulation, as an optimal parameter set, we determined the gear tooth number combination, module, and profile shift coefficient, (Table II), which achieved approximately 8 arcmin of backlash and 84% back-driving efficiency. Compared to bilateral drive [10], the gear teeth combinations changed overall, even for the same gear ratio (with a particularly significant change in the number of teeth for R_2). Moreover, the profile shift coefficients showed overall variation (especially for R_1 and R_2), and the module also exhibited significant differences.

V. EXPERIMENT

We developed a prototype 3K compound gearbox to evaluate the proposed design model. When evaluating the performances of the gearbox, the arrangement of sensors and actuators may change, but the fundamental components such as data acquisition system and power supplies that comprise it remain similar.

A. Backlash evaluation

To measure the backlash, we connected a powder brake (PRB Y-4 PORA ELECTRIC MACHINERY) to the output side and fixed it, while operating an electric motor (EC 90 frameless 260W MAXON) on the input side capable of continuously applying approximately 1 Nm, see Fig. 9 (a). Initially, the upper limit torque was defined, and the backlash was measured by gradually rotating in the positive direction at a sufficiently slow speed (~ 0.1°/s) and reversing the rotation

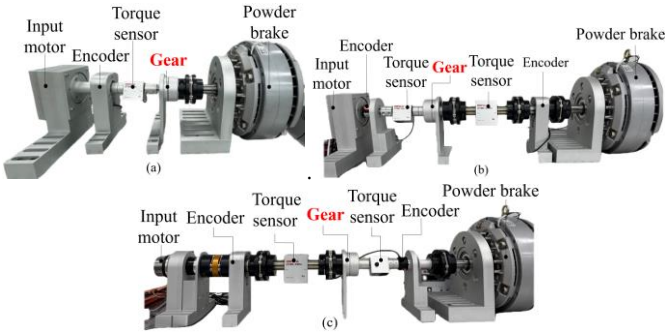

Fig. 9 Experimental setup for backlash with back-driving torque (a), forward drive efficiency (b), and backward drive efficiency (c).

upon nearing the upper limit torque. The criterion for determining the upper limit torque was the point at which the angle no longer changed. During this process, high-resolution encoder (MTL MEH-60) and torque sensor (UTMII-2Nm) were arranged to simultaneously acquire corresponding angle and torque. Fig. 10 represents the experimentally acquired torque-angle relations. We applied a zero-phase filter to the raw data. From the torque-angle relationship, the backlash was estimated by calculating the difference between the two angles at the points where the torque is zero. The experiment confirmed that it is approximately 7.1 (0.3) arcmin.

B. Backdrivability

We evaluated the back-drivability by measuring the backdriving torque of the developed gear. We used the same experimental setup as the backlash measurement and applied a sinusoidal input to rotate the output axis of the gear, as shown in Fig. 9 (c). The maximum back-driving torque was approximately 0.38 Nm. In addition, we selected the torque at the point where back-driving starts based on the measured torque, see Fig. 11. Upon checking the measured torque at the point where the output angle starts to change, we found it to be approximately 0.025 Nm which is referred to as 'back-drive starting torque' [10].

C. Bi-directional efficiency

1) Forward efficiency:

The experimental setup of measuring the forward drive efficiency is shown in Fig. 9 (b). We used the same input motor, input torque sensor, and powder brake as the setup of backlash with backdriving torque. For the input speed, an encoder (E40H100-5000-3-N-5, RLS, KOREA) with higher allowable speed (5000 rpm) was used. The output power at the gear box output stage was measured using the same encoder (MTL MEH-60) and high-capacity torque sensor (UTMII-200Nm) employed in the backlash measurement. The input angular velocity varied from 200 to 1000 rpm in steps of 200 rpm, while the load torque ranged from 5 to 50 Nm in steps of 15 Nm.

The forward efficiency was calculated as below.

$$\eta = \tau_o w_o / \tau_i w_i \tag{38}$$

where τ_i, w_i, τ_o, and w_o are the input torque, input angular velocity, output torque, and output angular velocity respectively. The experimental result showed that the maximum forward efficiency was approximately 87.1 %, see Fig. 12 (a).

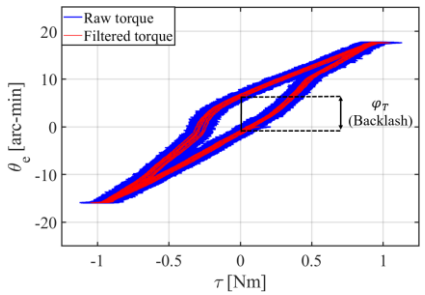

Fig. 10 (a) Torque-angle curve representing angular transmission error including backlash angle, φ_T.

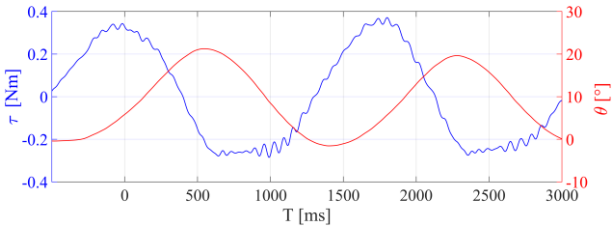

Fig. 11 (a) Measured back-driving torque, τ and the corresponding output position, θ.

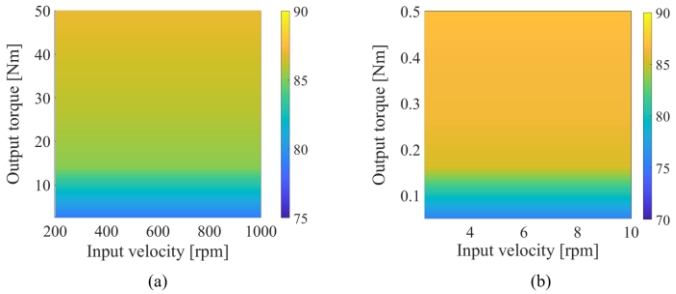

Fig. 12. Efficiency map of the forward drive (a) and backward drive (b) from the experiment.

2) Backward efficiency:

For the back-driving efficiency experiment, see Fig. 10 (b), an actuator with higher torque and lower speed compared to the input motor used in the forward drive efficiency experiment (EC 60 frameless 160W and with the Planetary Gearhead GP 52 C MAXON) was implemented. The high-torque capacity sensor (UTMII-200Nm) and the high resolution encoder (MTL MEH-60) was used as input torque sensor and encoder. The torque sensor (UTMII-2Nm) and the rotary encoder (E40H100-5000-3-N-5, RLS, KOREA) used at the input stage during the forward efficiency measurement were instead used to measure the output quantities in the backward efficiency measurement. The input angular velocity varied from 2 to 10 rpm in steps of 200 rpm, while the load torque ranged from 0.05 to 0.5 Nm in steps of 0.15 Nm. We also used a relation (38) for backward efficiency calculation. From the experimental data of the backward drive, the maximum backward efficiency was 82.5 %, see Fig. 12 (b).

VI. Discussion and Conclusion

This study presents the bi-directionally efficient, low-backlash and highly back-drivable gearbox design for robot actuator. Through detailed modeling and analysis of gear backlash in the 3K compound planetary gearbox, we

TABLE III
PERFORMANCE COMPARISON WITH OTHER GEARBOX

	Proposed	Bilateral drive [10]	Harmonic drive (CSG 25-LW) [5]
Gear ratio	96.2:1	96.2:1	100:1
Backlash [arc-min]	7.1	24	0.15
Back-driving starting torque [Nm]	0.025	0.02	11
Forward efficiency [%]	87.1	89.0	67.9
Backward efficiency [%]	82.5	85.3	N/A
Torque to weight ratio [Nm/kg]	118.3	90.2	79.1
Diameter [mm]	76	94	86

investigated the extent of the backlash improvement by maximizing the gear efficiency with changing the gear configuration compared to the motivated previous study [10]. We experimentally validated that the backlash was reduced from 24 arc-min to 7.1 arc-min. The proposed backlash model was confirmed to have high accuracy, achieving 99% and 98.5% when compared with the experimental data from previous studies and the prototype developed in this study, respectively. The measured forward and backward efficiency showed 87.1 % and 82.5 % respectively, which are comparable to the bilateral drive [10] efficiencies of 89 % and 85.3 %, respectively, as shown in Table III.

To the best of our knowledge, this is the first study to determine the effective inertia of the 3K compound planetary gearbox by considering the power balance during gear meshing. From the derived equations (32) and (33), we could verify that the effective inertia is not simply determined by the square of the overall gear ratio in inverse proportion but is instead influenced by the combination of each gear's rotational inertia, the gear ratio during each gear meshing, and, most importantly, the backward efficiency during each gear meshing. Above all, we argue that deriving a quantitative relationship between backward efficiency and effective inertia of backward drive holds significant importance, as it provides a foundation for direct application in design processes. Measured back-driving starting torque is approximately 0.025 Nm, a value that is substantially lower (~1/450) than that of harmonic drives typically used in robot actuators. Furthermore, it aligns closely with the performance of previously developed bilateral drives (0.02 Nm) [10], offering a significant benefit for robotics applications requiring a back-drivability for safety [22]. We expect this knowledge could serve as a guidance for gear design essential for robots that engage in physical interaction.

REFERENCES

[1] T. K. Best, G. C. Thomas, S. R. Ayyappan, R. D. Gregg and E. J. Rouse, "A Compensated Open-Loop Impedance Controller Evaluated on the Second-Generation Open-Source Leg Prosthesis," in *IEEE/ASME Transactions on Mechatronics*, doi: 10.1109/TMECH.2024.3508469.

[2] P. Slade, C. Atkeson, J. M. Donelan, H. Houdijk, K. A. Ingraham, 10 M. Kim, K. Kong, K. L. Poggensee, R. Riener, M. Steinert, J. Zhang, and S. H. Collins, "On human-in-the-loop optimization of humanrobot interaction," Nature, vol. 633, no. 8031, pp. 779–788, sep 2024.

[3] P. L. Garcia et al., "R2poweR: The Proof-of-Concept of a Backdrivable, High-Ratio Gearbox for Human-Robot Collaboration," 2022 International Conference on Robotics and Automation (ICRA), Philadelphia, PA, USA, 2022, pp. 01-07, doi: 10.1109/ICRA46639.2022.9811923.

[4] S. Zhang and P. Zhang, "Research on the mass unbalance response of an inner planetary gear reducer," in Proc. Int. Conf. Mechatronics Automat.,2009, pp. 3415–3419.

[5] Harmonic Drive AG. "Engineering data CSG-2A component sets," 2022. [Online].Available: https://harmonicdrive.de/fileadmin/user_upload/2014_11_ED_1019654_CSG-2A.pdf

[6] P. L. Garc´ıa, S. Crispel, E. Saerens, T. Verstraten, D. Lefeber, Compact gearboxes for modern robotics: A review, Frontiers in Robotics and AI 7 (2020) 103. doi:10.3389/frobt.2020.00103.

[7] W. Shin, G. Park, J. Lee, H. Chang and J. Kim, "Power Transmission Design of Fast and Energy-Efficient Stiffness Modulation for Human Power Assistance," 2021 IEEE International Conference on Robotics and Automation (ICRA), Xi'an, China, 2021, pp. 10877-10883, doi: 10.1109/ICRA48506.2021.9561044.

[8] A. Wang and S. Kim, "Directional efficiency in geared transmissions: Characterization of backdrivability towards improved proprioceptive control," 2015 IEEE International Conference on Robotics and Automation (ICRA), Seattle, WA, USA, 2015, pp. 1055-1062, doi: 10.1109/ICRA.2015.7139307.

[9] D. J. Braun, V. Chalvet and A. Dahiya, "Positive–Negative Stiffness Actuators," in *IEEE Transactions on Robotics*, vol. 35, no. 1, pp. 162-173, Feb. 2019, doi: 10.1109/TRO.2018.2872284.

[10] H. Matsuki, K. Nagano and Y. Fujimoto, "Bilateral Drive Gear—A Highly Backdrivable Reduction Gearbox for Robotic Actuators," in IEEE/ASME Transactions on Mechatronics, vol. 24, no. 6, pp. 2661-2673, Dec. 2019, doi: 10.1109/TMECH.2019.2946403.

[11] S. Oba and Y. Fujimoto, "Hybrid 3K Compound Planetary Reduction Gearbox With a Roller Transmission Mechanism," in *IEEE/ASME Transactions on Mechatronics*, vol. 27, no. 4, pp. 2356-2366, Aug. 2022, doi: 10.1109/TMECH.2021.3101236.

[12] A. Kawamoto, "Planetary roller type traction drive unit for printing machine," Koyo Engineering Journal, 165, pp. 60-64 (2004)

[13] S. NIDEC-SHIMPO CORPORATION, Traction Drive for Rotating Wheels High Precision AC Servo Actuator. Accessed: Jan. 28, 2021. [Online]. Available: http://www.nidec-shimpo.co.jp/

[14] S. Yu *et al*., "Quasi-Direct Drive Actuation for a Lightweight Hip Exoskeleton With High Backdrivability and High Bandwidth," in *IEEE/ASME Transactions on Mechatronics*, vol. 25, no. 4, pp. 1794-1802, Aug. 2020, doi: 10.1109/TMECH.2020.2995134.

[15] D. V. Gealy *et al*., "Quasi-Direct Drive for Low-Cost Compliant Robotic Manipulation," *2019 International Conference on Robotics and Automation (ICRA)*, Montreal, QC, Canada, 2019, pp. 437-443, doi: 10.1109/ICRA.2019.8794236.

[16] N. Kau, A. Schultz, N. Ferrante and P. Slade, "Stanford Doggo: An Open-Source, Quasi-Direct-Drive Quadruped," *2019 International Conference on Robotics and Automation (ICRA)*, Montreal, QC, Canada, 2019, pp. 6309-6315, doi: 10.1109/ICRA.2019.8794436.

[17] T-MOTOR, "AK80-6 Dynamical Modular," T-MOTOR Store. Accessed: Jan. 4, 2025. [Online]. Available: https://store.tmotor.com/product/ak80-6-dynamical-modular.html.

[18] ISO 21771: 2007 Gears — Cylindrical involute gears and gear pairs — Concepts and geometry, 2007.

[19] W. Shin, B. Ahn and S. Kwon, "A low backlash and highly efficient gearbox for robot actuator," *2024 IEEE International Conference on Advanced Intelligent Mechatronics (AIM)*, Boston, MA, USA, 2024, pp. 224-229, doi: 10.1109/AIM55361.2024.10637046.

[20] S. Crispel et al., "A novel wolfrom-based gearbox for robotic actuators," IEEE/ASME Transactions on Mechatronics, vol. 26, no. 4, Aug. 2021. DOI: 10.1109/TMECH. 2021.3079471.

[21] P. E. Gill and E. Wong, "Sequential quadratic programming methods," in Mixed Integer Nonlinear Programming, J. Lee and S. Leyffer, Eds. New York: Springer-Verlag, 2012, pp. 147–224, doi: 10.1007/978-1-4614-1927-3_6.

[22] Y. J. Kim, "Anthropomorphic low-inertia high-stiffness manipulator for high-speed safe interaction," IEEE Transactions on Robotics, vol. 33, no. 6, pp. 1358–1374, Dec. 2017, doi: 10.1109/TRO.2017.2732354.